

# Data report: particle size analysis of sediments recovered during IODP Expeditions 315 and 316, Sites C0001–C0008, Nankai Trough forearc, off Japan<sup>1</sup>

Achim Kopf,<sup>2</sup> Michael Strasser,<sup>2</sup> Nils Monsees,<sup>2</sup> Michael B. Underwood,<sup>3</sup> and Junhua Guo<sup>3</sup>

## Chapter contents

<a href="#">Abstract</a> .....	1
<a href="#">Introduction</a> .....	1
<a href="#">Geological setting</a> .....	2
<a href="#">Methods</a> .....	4
<a href="#">Results</a> .....	6
<a href="#">Discussion and conclusion</a> .....	7
<a href="#">Acknowledgments</a> .....	8
<a href="#">References</a> .....	8
<a href="#">Figures</a> .....	11

## Abstract

The Nankai Trough Seismogenic Zone Experiment is a multiexpedition project carried out in several stages by the Integrated Ocean Drilling Program. The first stage of the experiment included two cruises during which coring took place (Expeditions 315 and 316). We have studied grain size distribution in more than 600 specimens of cores from Sites C0001, C0002, C0004, and C0006–C0008 and correlated the distributions to the lithologies recovered, logging and logging-while-drilling data in nearby holes, and the overall tectonic setting. The two sites in the upper slope and Kumano Basin (Sites C0001 and C0002, respectively) show the smallest mean grain sizes, which are smaller in the accreted strata compared to the forearc basin or slope sediments. Further downslope (Sites C0004 and C0008), grain size variability is larger and lithologies range from slope apron, mass transport deposits, accreted mud/mudstones, and fault zone material, to underthrust hemipelagics. Surprisingly, the mass transport deposits at Site C0004 are fine grained, whereas their counterparts at Site C0008 slightly downslope are the coarsest within the recovered succession there. The two sites near the toe of the accretionary prism (Sites C0006 and C0007) provided the coarsest material recovered, namely the trench–slope transition facies and the uppermost accreted trench wedge facies. Mudstones from the underlying upper Shikoku Basin facies are well sorted, uniform, and fine grained.

In general, the study provides a solid basis for more specialized sedimentological research and further reveals that (1) results of the measurements taken with the Coulter Counter LS200 laser particle analyzer are in good agreement with earlier onboard visual core description; (2) accuracy and reproducibility of the method is satisfactory given the very narrow error bars of repeat measurements on aliquots of a larger sediment sample; and (3) the mass transport deposits have distinct particle size distribution patterns, whereas fault gouge and other material from structural features cannot easily be distinguished from surrounding sediment by grain size analysis alone.

## Introduction

The systematic investigation of particle size distribution of clastic sediments dates back to benchmark studies by, for example, Udden (1914), Wentworth (1922), Spencer (1963), and Folk (1966). More recently, grain size analysis of large populations of sediment

<sup>1</sup>Kopf, A., Strasser, M., Monsees, N., Underwood, M.B., and Guo, J., 2011. Data report: particle size analysis of sediments recovered during IODP Expeditions 315 and 316, Sites C0001–C0008, Nankai Trough forearc, off Japan. In Kinoshita, M., Tobin, H., Ashi, J., Kimura, G., Lallemand, S., Screaton, E.J., Curewitz, D., Masago, H., Moe, K.T., and the Expedition 314/315/316 Scientists, *Proc. IODP, 314/315/316*: Washington, DC (Integrated Ocean Drilling Program Management International, Inc.).  
doi:10.2204/iodp.proc.314315316.207.2011

<sup>2</sup>Center for Marine Environmental Sciences (MARUM), University of Bremen, D-28359 Bremen, Germany. Correspondence author: [akopf@uni-bremen.de](mailto:akopf@uni-bremen.de)

<sup>3</sup>Department of Geological Sciences, University of Missouri, Columbia MO 65211, USA.



samples obtained with modern and fast instruments has found an important application in the study of sedimentary processes and their environmental significance (Stow and Wetzel, 1990; Weedon and McCave, 1991; Jones et al., 1992; Lucchi and Camerlenghi, 1993; Rothwell et al., 1994; Sutherland and Lee, 1994).

The Integrated Ocean Drilling Program (IODP) Nankai Trough Seismogenic Zone Experiment (NanTroSEIZE) complex drilling project defines as one of its foremost objectives to shed light on the changes in physical properties and stress state of the Nankai Trough plate boundary thrust as well as prominent out-of-sequence thrusts (OOSTs) splaying off this detachment surface (Tobin and Kinoshita, 2006). On board the D/V *Chikyu*, no apparatus for grain size measurements exists. As a consequence, the systematic study of particle size distributions along the NanTroSEIZE transect of drill sites off the Kii Peninsula (Fig. F1) is hampered. On the other hand, such a study, when combined with X-ray diffraction (XRD) analysis, seems crucial to unraveling how particle size and mineralogical composition influence the onset of faulting at the toe of the accretionary prism and within the incoming sedimentary sequence and further downdip along the plate boundary thrust (see similar work in western Nankai [Brown et al., 2003], central Nankai [Kopf and Brown, 2003; Underwood et al., 2003], Barbados [Deng and Underwood, 2001], and Costa Rica [Spinelli and Underwood, 2004]). In this short manuscript we show results from particle size analyses of a large number (>600) of sediment samples from all NanTroSEIZE Stage 1 drill sites where coring took place (see Tobin et al., 2009a). These data hopefully will become an important component in future manuscripts concerning sediment-tectonic stratigraphy and processes, but also the physical properties and mechanical response of fault zone materials and surrounding hanging wall and footwall sediments.

## Geological setting

### The Nankai accretionary prism along the Kumano Transect

Along the Nankai Trough subduction system, a large accretionary complex off the coast of southwest Japan has been accumulated as a result of the Philippine Sea plate being subducted beneath the Eurasian plate at a rate of ~4 mm/y (Fig. F1A). The several hundred kilometer wide accretionary wedge consists of mainly trench-fill turbidites and incoming Shikoku Basin hemipelagic sediments that were off-scraped from the downward moving plate. This study covers the central portion of the Kumano

transect (Fig. F1B), which was recently extended both landward and seaward during NanTroSEIZE Stage 2 drilling (Expedition 319 Scientists, 2010; Underwood et al., 2010). The transect is divided into six main morphotectonic zones, which are, from southeast to northwest, trench, frontal thrust zone (FTZ), imbricated thrust zone (ITZ), megasplay fault zone (MSFZ), Kumano Basin edge fault zone (KBEFZ), and the Kumano forearc basin (Moore et al., 2009).

In the trench zone, younger trench deposits, the so-called trench wedge facies, overlie the oceanic crust and Shikoku Basin sediments (Fig. F1B). Farther landward, a well-developed prototrust zone has developed; however, it is overlain by a slice of trench strata previously accreted into the prism and emplaced over the trench strata by an OOST (see the “Expedition 316 summary” chapter [Screaton et al., 2009a]; Moore et al., 2009; Screaton et al., 2009b). The FTZ appears highly complex with a very steep slope (~10°) and a large embayment interpreted as slump scar possibly reflecting indentation by a recently subducted seamount (Screaton et al., 2009b). The deposits of this prism-toe collapse are found as irregular hummocky bathymetry seaward of the embayment, where the trench channel has been deflected significantly, likely caused by blockage of axial flow by mass-wasting deposits (Kawamura et al., 2010).

Landward of the prism front is the ITZ a series of thrust packages reflecting past in-sequence thrusting and accretion. The ITZ is overlain by slope sediments deposited in slope basins within the ridge-basin topography typical of fold-and-thrust belts developed in many accretionary prisms (e.g., Morley, 2009). The thickness of these basins generally increases landward from southeast to northwest (Fig. F1B). Beneath the upper slope and Kumano Basin, a regional splay fault system, first recognized by Park et al. (2002) and later termed “megasplay” by Tobin and Kinoshita (2006), discontinuously cuts across the older part of the accretionary prism and intersects its shallow landward edge (Moore et al., 2007; Moore et al., 2009). The shallow part of the MSFZ is a complex thrust system with backward breaking branches that truncate the imbricate thrust faults within the accretionary prism and override younger slope basin sediments (Moore et al., 2007; Strasser et al., 2009). Landward of the MSFZ, along the forearc high, the Kumano forearc basin is bounded on the southeast by a topographic valley. Beneath the valley is a complex fault zone that may comprise a combination of normal and strike-slip faults (KBEFZ; Martin et al., 2010). More than 2 km of sediment is imaged in the Kumano forearc basin. The seaward portion of the basin section is progressively tilted and dips landward, likely because of repeated motion on the

megasplay fault (Park et al., 2002). New data by Gulick et al. (2010) point toward a major phase of landward tilting of sediment packages and inferred megasplay activity between 1.3 and 1 Ma that post-dates an earlier phase of asymmetric forearc high uplift (more uplift in southwestern part of the Kumano transect) that may have occurred in concert with splay fault steepening and underthrusting of a large volume of sediment beneath the thrust (Bangs et al., 2009). In the shallow subsurface deposits, however, evidence for soft-sediment deformation and submarine landslides exists in the steeper portion of the slope (Kawamura et al., 2009; Strasser et al., 2011).

### Lithostratigraphic summary of Sites C0001–C0008

During IODP Expedition 315, coring at Sites, C0001 and C0002 took place (Fig. F1B). Drilling at Site C0001 cored to 458 meters below seafloor (mbsf) and 60 cores, 32 with the hydraulic piston coring system (HPCS), 2 with the extended shoe coring system (ESCS), and 26 with the rotary core barrel (RCB), were collected from five holes covering the slope basin (lithologic Unit I) and the uppermost 250 m of the underlying accretionary prism (Unit II). The slope basin is composed mainly of Quaternary to late Pliocene silty clay and clayey silt with intercalations of volcanic ash. The boundary between Units I and II was identified at 207 mbsf and represents an unconformity located immediately below a thick sand layer (Fig. F2; left column). Unit II is composed of mud-dominated sediments of late Pliocene to late Miocene age (see the “Expedition 315 summary” chapter [Ashi et al., 2009]).

At Site C0002, a total of depth of 1057 mbsf was reached, with cored intervals from 0 to 204 and 475 to 1057 mbsf and 86 cores cut, 18 cored with the HPCS, 2 with the ESCS, and 66 with the RCB, from three holes. The basal unconformity of the Kumano forearc basin was drilled at ~922 mbsf and cored another 135 m into the accretionary prism. The forearc basin sequence was divided into two lithologic units based on lithofacies. The boundary core between lithologic Units I and II was not recovered; hence, the logging unit boundary defined by logging-while-drilling (LWD) during IODP Expedition 314 was applied for this boundary. All units (i.e., Units I–IV) are dominated by mud and mudstone; however, Units I and II contain more sand and silt intercalation and have a much faster sedimentation rate. The age ranges from Quaternary to late Miocene. Units I and II are Quaternary deposits, whereas the underlying basal basin units are comprised of hemipelagic mud of Pliocene age (Fig. F3; left column). These sediments are underlain by accretionary prism materials

containing moderately more lithified and much more deformed sediments (Unit IV). Biostratigraphic data show that the transition from Pliocene to late Miocene strata occurs as a gap around 922 mbsf, ~15 m above the lithologic unit boundary defined during Expedition 314 based on LWD data (see the “Expedition 314 summary” chapter [Tobin et al., 2009b]). Faults and shear zones are frequently observed in the core and clustered at several depths around 700, 920–950, and 1000–1050 mbsf.

IODP Expedition 316 was designed to evaluate the deformation, inferred depth of detachment, structural partitioning, fault zone physical characteristics, and fluid flow at the frontal thrust and at the shallow portion of the megasplay system. To accomplish these objectives, drilling was conducted at two sites in the megasplay region (Sites C0004 and C0008), one within the fault zone and one in the slope basin seaward of the MSFZ. Two sites (C0006 and C0007) were also drilled within the FTZ and protothrust zone (PTZ) (Fig. F1B) (see the “Expedition 316 summary” chapter [Screaton et al., 2009a]).

Site C0004 is located along the slope of the accretionary prism landward of the tip of the megasplay fault zone. Drilling at this site examined the youngest hemipelagic sediments on the slope (interpreted to be early to late Pleistocene) overlying the accretionary prism. These accreted sediments consist of slowly deposited marine sediments and redeposited material from upslope and were deposited during the late to middle Pliocene (Fig. F4; left column). This redeposited material consists mainly of sedimentary breccia and was interpreted as a mass transport complex (MTC) with silty clay clasts that most likely result from deposition of slumps along an unstable slope. The dominant lithology here is dark greenish gray silty clay. The accretionary prism (middle Pliocene) was sampled, and the MSFZ was successfully drilled. The top of the prism corresponds to a prominent unconformity (age gap = ~1 m.y.) that displays mineralization by pyrite and other minerals. Structural observations of core material from the fault zone and two age reversals suggested by nannofossils indicate a complex history of deformation and the presence of multiple imbricated sediment packages. Sediments under the fault zone were sampled to understand their deformation, consolidation, and fluid flow history. This succession (lithologic Unit IV; 307 mbsf to the bottom of Hole C0004D at 403 mbsf) (Fig. F4) is early Pleistocene in age and consists of dark olive-gray silty clay with a moderate amount of calcareous nannofossils and a lesser amount of calcareous and siliceous microfossils. Thin sand and silt beds are common in this unit, particularly in the uppermost part. It is interpreted to have formed in a lower trench-slope basin, dominated by fine-grained

hemipelagic deposition with relatively minor sand input (for details, see the [“Expedition 316 Site C0004”](#) chapter [Expedition 316 Scientists, 2009a]).

Drilling at Site C0008 targeted the slope basin seaward of the megasplay fault. This basin records the history of megasplay fault movement. In addition, sediment layers within this basin provide a reference for sediment underthrusting the splay fault zone at Site C0004. Two lithologic units were identified at Site C0008. The uppermost unit (lithologic Unit I) consists of a 272 m (in Hole C0008A) succession of hemipelagic silty clay with thin sand beds and volcanic ash layers. In addition to the discrete ash layers, volcanic glass and pumice are disseminated as a significant component within the sediments. At the base of Unit I, a 40 m section of clayey gravel containing rounded clasts of mudstone and pumice constitutes Subunit IB. This subunit is interpreted as a MTC accumulated in the lower slope basin, possibly during an early stage of basin formation. The Pleistocene/Pliocene boundary is found within Subunit IB. Unit II includes ~57 m of sand-rich sediment for which there was very limited recovery. This sand, along with a minor gravel component, contains a diverse detrital grain assemblage that includes clasts of sedimentary, metasedimentary, plutonic, and volcanic rocks (see the [“Expedition 316 Site C0008”](#) chapter [Expedition 316 Scientists, 2009d]).

Drilling at Sites C0006 and C0007 allowed examination of the frontal thrust region. At Site C0006, coring was completed to 603 mbsf before poor hole conditions stopped drilling prior to reaching the frontal thrust. Three lithologic units were recognized: Unit I is Pleistocene–Holocene in age; extends from the seafloor to 27 mbsf; and consists of a fining-upward succession of silty clay, sand, silty sand, and rare volcanic ash layers. Unit II (27–450 mbsf) is Pleistocene in age and is interpreted as having been deposited in a trench setting. It contains dark gray to black fine-grained sand consisting dominantly of metamorphic and volcanic lithic fragments with secondary quartz and feldspar but also finer sand, silty sand, and silty clay. According to shipboard core description, individual sand beds (~1–7 m thick) typically grade into silt and occasionally silty clay with indistinct boundaries between the different lithologies (see the [“Expedition 316 Site C0006”](#) chapter [Expedition 316 Scientists, 2009b]). Unit III is late Miocene–early Pliocene in age and consists of greenish gray silty clay with some interbedded volcanic ash, including dolomite- and calcite-cemented ash. Unit III has overall increased clay content and decreased quartz and feldspar contents compared to the overlying sediments. Unit III was deposited by hemipelagic settling along with accumulation of volcanic ash. The Miocene–early Pliocene age and lithologic content of

Unit III are similar to the Shikoku Basin facies documented at Ocean Drilling Program (ODP) Sites 1173 and 1174 in the Muroto transect more than 100 km west-southwest along the Nankai Trough (e.g., Moore et al., 2001). A broad fractured/brecciated zone extending from 230 to 545 mbsf and commonly strongly fractured, striated, or with polished planes suggests that several fault strands within the prism were penetrated before drilling had to be stopped because of unfavorable hole conditions (see the [“Expedition 316 Site C0006”](#) chapter [Expedition 316 Scientists, 2009b]).

The plate boundary frontal thrust was successfully drilled, and thrust fault material ranging from breccia to fault gouge was successfully recovered at Site C0007. In summary, four lithologic units were identified. The uppermost unit (lithologic Unit I; 0–33.94 mbsf) consists of hemipelagic silty clay with interbedded sand. Deposition of this unit is interpreted to have occurred on the lowermost slope above the trench floor by hemipelagic settling, turbidite deposition, and possibly subsequent soft-sediment slumping on an oversteepened slope. Unit II extends to ~362 mbsf and constitutes a coarsening-upward succession from fine-grained mud to sand- and gravel-rich deposits. Biostratigraphy suggests a possible age reversal below 135 mbsf in Hole C0007C (within Unit II) and a significant age gap between Units II and III (see the [“Expedition 316 Site C0007”](#) chapter [Expedition 316 Scientists, 2009c]). Unit III (362–439 mbsf) is a Pliocene succession of green bioturbated fine-grained hemipelagic sediments. Thin (<1 cm) greenish layers, reworked glauconite, and pervasive burrowing suggest that low sedimentation rates accompanied the deposition of this lowermost mud. Underneath, the significantly younger deposits (Pleistocene) of Unit IV may be correlated on seismic profiles with the active trench wedge of the Nankai Trough further southwest, an observation that is supported by enhanced drilling rates in the fine- to medium-grained sands. Fault zones at 237–259 mbsf (Fault Zone 1) and 341–362 mbsf (Fault Zone 2) are located at depths of lithologic changes. For detailed description, see the [“Expedition 316 Site C0007”](#) chapter (Expedition 316 Scientists, 2009c).

## Methods

Samples were analyzed at the Center for Marine Environmental Sciences (MARUM) in Bremen, Germany, using standard laser diffraction analysis. This method was chosen because we have considerable experience using this technique on fine-grained sediment. The technique is sufficiently versatile to process a large number of samples using an Auto-Prep Station with no minimum particle size restrictions.

## Principles of laser diffraction analysis

Laser diffraction size analysis is based on the principle that particles of a given size diffract light through a given angle, the angle increasing with decreasing particle size (see the superb summary by Syvitski, 1991, and references therein). A narrow beam of monochromatic light ( $\lambda = 750$  nm) is passed through a sample cell containing an upward moving suspension. The diffracted light is focused onto 126 detectors. To calculate the grain-size distribution from the light intensity reaching the array of detectors, two different diffraction theories can be used. We used the Fraunhofer theory because Loizeau et al. (1994) concluded that this detects a significantly larger proportion of the clay measured by the sieve-pipette method than does the Mie theory. The Fraunhofer theory starts from the principle that there is only diffraction and no refraction; this is not entirely correct for organic matter because it may absorb some light. If particles are large compared to the wavelength of the light, the interaction can be interpreted in terms of diffraction (de Boer et al., 1987). The wavelength of the laser light therefore suggests that measurement of the clay fraction may be problematic. The size distribution is measured while the suspension is subject to continuous pumping. This ensures random orientation of most particles relative to the laser beam so that the equivalent spherical cross-sectional diameter is measured.

The Coulter LS-13320 measures grain size contents in 117 classes ranging from 0.04 to 2000  $\mu\text{m}$  as a volume percent (vol%) (see more detailed discussion by Syvitski et al., 1991, and Loizeau et al., 1994). Water, which was degassed before analysis, was used as suspension fluid. Each run took 60 s and was repeated 5 times. The third run is used as statistical representative run for data quality control.

We chose the laser technique over Sedigraph grain size analysis because the latter is not capable of measuring particles  $<10$   $\mu\text{m}$  (e.g., Konert and Vandenberghe, 1997), which in a setting such as the Nankai Trough accretionary prism would pose problems because of the substantial clay fraction. An comparison between the two (and other) techniques is difficult, as has been pointed out by several authors (see Syvitski et al., 1991, and references therein). Definition of accuracy has been attempted in some of these studies, but no coherent conclusion can be drawn from the wealth of different results. However, it is beyond the scope of this paper to elaborate on the various grain size standards available and how they compare when run on different machines, not to mention which of them is best. The main argument for using the Coulter counter laser apparatus was the time efficiency, large range, and very high reproducibility of the measurements (see below).

## Samples

Two types of samples were used in this study: XRD and fabric (FAB). FAB samples are normal cluster samples next to the whole-round sample intervals including interstitial water. The whole-round intervals were positioned within intact hemipelagic mud (and/or mudstone) and are leftover material after processing for clay XRD.

### Sample preparation and handling

The samples were removed from the plastic sample bag to weigh an aliquot. In order to get a statistically representative subsample it was necessary to remold a larger volume of unconsolidated and partly consolidated material. Approximately 0.15 g of a sample was first disaggregated by boiling with 50 mL degassed water and  $\sim 0.1$  g of sodium pyrophosphate ( $\text{Na}_4\text{P}_2\text{O}_7 \cdot 10\text{H}_2\text{O}$ ) in a beaker. This agent dissolves at  $\sim 80^\circ\text{C}$  and supports the disaggregation of agglomerated particles in suspension (Sun et al., 2002). After boiling, the samples were put in an ultrasonic bath for at least 30 min. The ultrasonic bath is capable of hosting eight beakers at a time. After 30 min, the samples were shaken by hand (using the same beaker) to test if all particles were in suspension. If there were still some aggregates on the bottom of the beaker, the samples were placed again in the ultrasonic bath for 30 min. The samples were taken out of the ultrasonic bath and put aside for at least one day to let the particles settle.

A portion of the sample ( $\sim 5$  mL) was then aspirated to a test tube with a suction device to use in the Auto-Prep Station. The wheel inside this station can handle 30 samples in one batch.

Grain size was measured with a Coulter LS200 counter on bulk material, resolving grain size spectra between 0.4 and 2000  $\mu\text{m}$ .

In order to check for accuracy and comparability of results to data obtained with different machines in other laboratories, we regularly run grain standards by Retsch and Coulter.

### Data acquisition, processing, and statistics

The Beckman Coulter LS program used for the measurements offers an interface to set up batches and automatically saves the produced data in separate  $.\text{LS}$  files for each run. Every third run was manually copied into an Excel file calculate statistics in quasi-real time. Mean grain sizes were calculated with GRADISTAT software (Blott and Pye, 2001) after the Folk and Ward (1957) method (i.e.,  $M$  being an average value taking into account the grain sizes at the 16th, 50th, and 84th percentiles). Sorting (i.e., the standard deviation) and skewness, used as measures

for the width and symmetry in the 117 grain size classes, were also calculated based on the formulas given in Folk and Ward (1957).

## Results

The grain size distribution from specimens recovered at Sites C0001, C0002, C0004, and C0006–C0008 is presented as volumetric fractions of clay, silt, and sand next to the lithostratigraphic columns (Figs. F2, F3, F4, F5, F6, F7) and as variation of mean grain size versus depth (Fig. F8). Note that we do not present the data in consecutive order with respect to site numbering (i.e., the chronological order of drilling) but as a function of their position across the accretionary margin. Sites C0001 and C0002 represent the upper slope and seaward forearc basin, Sites C0004 and C0008 are in the mid-slope, whereas Sites C0006 and C0007 are at the lowermost slope near the frontal portion of the accretionary wedge (Fig. F1B).

At Site C0001, the grain size distribution of lithologic Units I and II is fairly similar, with the former being somewhat coarser than the latter (Fig. F2). On average, sand content in the slope apron deposits (Unit I) reaches ~5%, with maximum values reaching 12% in the silty turbidite sequence near the unconformity. Below the unconformity, the accreted, sometimes bioturbated, muds of Unit II are generally <5% sand (Fig. F2). Silt is the dominant grain size class in both units, whereas clay is ~40% (Unit I) and 45% (Unit II).

Further landward (northwest) at Site C0002, grain size data were collected only for three of the four lithologic units drilled (Fig. F3). No data exist for the Quaternary sediments of Unit I in the upper Kumano Basin sequence. In the lower forearc basin sediments, silt is the dominant grain size, whereas sand approaches and occasionally exceeds 10% and clay may be as low as 20% in places (largely in the coarser turbidite layers that are interbedded within the hemipelagic mud). Unit III represents the basal forearc basin facies of predominantly Pliocene age, where a gradual increase in clay fraction is observed (from ~30% to ~50%; see Fig. F3). Sand content from either turbidites or ash ranges between 5% and 15%. In Unit IV, representing the uppermost accreted sediment, the sand fraction drops to a nearly constant 5% (exceptions are occasional thin turbidite beds). Silt accounts for ~50% of the particles, whereas clay content is lower than in Unit III (Fig. F3).

When moving to the southeast and down the slope, the shallow sedimentary succession changes drastically. At Site C0004 (Fig. F4), the 78 m thick slope apron sediments are still clayey (~30%–40%) silt (~50%–60%) with occasional fine sand or ash layers

(usually <5% sand fraction). Just below (see the “[Expedition 316 Site C0004](#)” chapter [Expedition 316 Scientists, 2009a]), a 40 m thick MTC (Subunit IIA) comprising sedimentary breccia and hemipelagic muds was recovered. If the individual clasts are disregarded for grain size analysis, the overall pattern in this unit is fairly homogeneous: ~45% clay, ~55% silt, and ~5% sand (Fig. F4). With the exception of a prominent ash layer at ~130 mbsf, Subunit IIB has an extremely similar grain size distribution as Subunit IIA. Unit III, the fault-bounded package separating the upper accretionary prism from the underthrust slope apron of Quaternary age, shows some scatter in the clay-silt range but has otherwise a similar grain size distribution as Unit II (Fig. F4). Finally, Unit IV shows a coarsening in overall grain size, with sand content up to 10%, silt content at 50% or slightly higher, and clay decreasing from ~40% to 30%–35%. Not unexpectedly, the underthrust slope apron (Unit IV) mimics the uppermost deposits (slope apron in Unit I) regarding both the grain size distribution and scatter (Fig. F4). The fault zone in Unit III, which represents the updip end of one branch of the megasplay fault, is somewhat finer grained than the other units (Fig. F4). However, it is coarser grained than what may be expected from potential particle disaggregation, cataclasis, and similar processes that are usually associated with large strains.

At Site C0008, adjacent to Site C0004 but a little further downslope, the entire grain size spectrum with depth shifted to coarser sizes. The slope apron (Subunit IA) largely ranges between 20% and 50% clay, ~30%–60% silt, and up to 30% sand (Fig. F5). Interestingly, the mass transport complex at this location (termed Subunit IB because, in contrast to Site C0004, the MTC deposits are within the slope basin unit; see the “[Expedition 316 Site C0008](#)” chapter [Expedition 316 Scientists, 2009d]) is coarser grained and further shows an increase in sand toward its base. Just below, Unit II represents the accreted trench wedge facies, where sand dominates over mud and recovery was poor, which may be taken as indirect evidence for the occurrence of sand. Since we tried to exclude individual clasts and other deposits of secondary (i.e., mass wasting) origin, we assume that the coarsening may be explained by amalgamation of trench wedge facies during emplacement.

When regarding the frontal portion of the accretionary wedge, two nearby sites were aimed at intersecting the frontal thrust (Sites C0006 and C0007; Fig. F1B).

At Site C0006, the uppermost ~600 m of sediment material was penetrated (Fig. F6). The uppermost ~30 m corresponds to lithologic Unit I, where hemipelagic mud with minor sand (10% ± 5% on average, with one interval containing up to 30%) were inter-

preted as trench–slope transitional deposits. The clay volume is 35% on average, and silt dominates (~55%–60%). Unit II (~30–450 mbsf) consists of accreted trench wedge sediment (Fig. F6), with the uppermost part to ~320 mbsf characterized by substantial scatter. Clay is  $40\% \pm 15\%$ , silt ranges from ~55% to  $60\% \pm 10\%$ , and sand is absent to  $>40\%$ . In the lowermost portion of Unit II, the variability in grain size is less pronounced, the sand fraction is almost negligible, and clay steadily increases from 40% at ~320 mbsf to 50% at 450 mbsf (Fig. F6). The lowermost Unit III, the upper Shikoku Basin facies, is characterized by fairly homogeneous mudstones with generally  $>50\%$  clay, 45% silt, and very little sand-sized material (often tephra). Although several structural features (e.g., shear bands) were penetrated by drilling in this unit, there is no systematic textural relationship between these thrust zones at this sampling scale.

The seawardmost drilling location cored during NanTroSEIZE Stage 1 was Site C0007 (Fig. F7) (see the “Expedition 316 Site C0007” chapter [Expedition 316 Scientists, 2009c]). Given the proximity to Site C0006, it is not surprising to find many similarities in the grain size patterns. Lithologic Unit I, comprising the trench–slope transition, shows a wide scatter with  $20\%–35\% \pm 8\%$  clay, a more or less steady 55% silt, and  $5\%–35\%$  sand (Fig. F7). In the accreted trench wedge facies below this interval, we observe again a larger scatter in texture in the upper portion and more uniform patterns in the lower portion. Unit II spans from ~30 mbsf to an unconformity at 362 mbsf, with substantial variability in texture to ~200 mbsf. Similar to Site C0006, the lower portion has increasing clay (up to 50%), a constant 50%–60% silt, and only occasional sand beds (Fig. F7). In Unit III, the upper Shikoku Basin facies, mudstones with clay fractions slightly exceeding 50% and little sand (0%–10%) are found. The scatter seen in the data does not correlate with any structural observations but merely reflects somewhat increased sand or ash contents in some intervals. In the accreted trench wedge facies underneath (Unit IV), recovery was insufficient to regularly sample the core for a continuous grain size record with depth (Fig. F7).

In Figure F8, we show the variation in mean grain size ( $\phi$ ) (sensu Folk and Ward, 1957) and grouped the six drill sites with respect to their position in the accretionary complex (Fig. F1B).

Sites C0001 and C0002 show fairly homogeneous curves with  $\phi$  ranging predominantly between 4–7  $\mu\text{m}$  (Site C0001) and 4–12  $\mu\text{m}$  (Site C0002) (Fig. F8). Mean grain size is larger in the slope apron and forearc basin when compared to the upper accretionary mud and mudstones.

When moving downslope,  $\phi$  at Site C0004 ranges mostly from 4 to 6  $\mu\text{m}$ , with the exception of the coarser, lowermost part of the underthrust slope apron, whereas Site C0008 is coarser ( $\phi = 5–12 \mu\text{m}$ ). Interestingly, the MTC at Site C0008 shows a much larger mean value (up to  $>20 \mu\text{m}$ ), whereas the MTC at Site C0004 exhibits the opposite trend with  $\phi$  close to 4  $\mu\text{m}$  in this interval (Fig. F8).

Near the toe of the accretionary complex, Sites C0006 and C0007 show the largest mean values of this study. In either location, Unit II (accreted trench wedge)  $\phi$  is  $>70 \mu\text{m}$  (Site C0006) and 90  $\mu\text{m}$  (Site C0007) in the upper portion (Fig. F8). In the lower portion of Unit II, the mean values drop drastically and  $\phi$  approaches 4  $\mu\text{m}$ , a value which is also typical for the mudstones of Unit III (upper Shikoku Basin facies).

All data of this study will be part of an electronic appendix that will be uploaded to the IODP Web site as well as the World Data Centre WDC-MARE ([www.pangaea.de](http://www.pangaea.de)) and can be used by other NanTroSEIZE researchers. See PARTSIZE in “Supplementary material.”

## Discussion and conclusion

Rather than focusing on the detailed sedimentological processes along the NanTroSEIZE drilling transect, we aim to provide some quality assessment concerning the basic grain size data set presented.

Apart from the routine triplicate runs and their statistical analysis, we also dedicated analyses to assess the overall performance of the Coulter Counter LS200. Figure F9 illustrates results from 16 aliquots of the same core sample. A batch of eight aliquots of the first half of the sample were dispersed in the ultrasonic bath for 60 min plus 48 h of particle settling (Fig. F9A), whereas the second batch of eight samples were dispersed for only 30 min with 24 h of settling time (Fig. F9B). The data of all 16 samples show near-perfect agreement in the fine-grained (i.e., clay size) part of the spectrum and some minor deviations from 6  $\mu\text{m}$  and above. Otherwise, the variability within the two batches was negligible, whereas the deviations between the two batches can be found. In fact, mean and median grain sizes of the specimens are shifted toward smaller values when time for disaggregation was increased. However, some of these differences in mean, median, and sorting (standard deviation) may be explained by initial differences when subsampling the specimen (i.e., minor natural variation within the sample chosen) and not so much from the treatment and grain size measurement.

In conclusion, the main findings of our study are as follows:

- Precision and reproducibility of the method are satisfactory given the very narrow error bars of repeat measurements on aliquots of a larger sediment sample.
- Results of the measurements with the Coulter counter LS200 laser particle analyzer are in good agreement with earlier shipboard qualitative visual core description.
- The mass transport deposits have distinct particle size distribution patterns, whereas fault gouge and other material from structural features cannot easily be distinguished from surrounding sediment by grain size analysis alone.

## Acknowledgments

This research used samples and data provided by the Integrated Ocean Drilling Program (IODP). Funding for participating in Expeditions 315 (to A. Kopf) and 316 (to M. Strasser) was provided by the German Science Foundation (DFG). Grain size analyses were also supported by DFG through MARUM Research Centre. Jan-Berend Stuut and Inka Meyer are thanked heartily for their assistance in the laboratory. The US National Science Foundation and IODP-Management International, Inc., are thanked for funding M.B. Underwood (Expedition 315 as well as specialty coordinator).

## References

- Ashi, J., Lallemand, S., Masago, H., and the Expedition 315 Scientists, 2009. Expedition 315 summary. *In* Kinoshita, M., Tobin, H., Ashi, J., Kimura, G., Lallemand, S., Screamton, E.J., Curewitz, D., Masago, H., Moe, K.T., and the Expedition 314/315/316 Scientists, *Proc. IODP*, 314/315/316: Washington, DC (Integrated Ocean Drilling Program Management International, Inc.). [doi:10.2204/iodp.proc.314315316.121.2009](https://doi.org/10.2204/iodp.proc.314315316.121.2009)
- Bangs, N.L.B., Moore, G.F., Gulick, S.P.S., Pangborn, E.M., Tobin, H.J., Kuramoto, S., and Taira, A., 2009. Broad, weak regions of the Nankai Megathrust and implications for shallow coseismic slip. *Earth Planet. Sci. Lett.*, 284(1–2):44–49. [doi:10.1016/j.epsl.2009.04.026](https://doi.org/10.1016/j.epsl.2009.04.026)
- Blott, S.J., and Pye, K., 2001. GRADISTAT: a grain size distribution and statistics package for the analysis of unconsolidated sediments. *Earth Surf. Processes Landforms*, 26(11):1237–1248. [doi:10.1002/esp.261](https://doi.org/10.1002/esp.261)
- Brown, K.M., Kopf, A., Underwood, M.B., and Weinberger, J.L., 2003. Compositional and fluid pressure controls on the state of stress on the Nankai subduction thrust: a weak plate boundary. *Earth Planet. Sci. Lett.*, 214(3–4):589–603. [doi:10.1016/S0012-821X\(03\)00388-1](https://doi.org/10.1016/S0012-821X(03)00388-1)
- de Boer, G.B.J., de Weerd, C., Thoenes, D., and Goossens, H.W.J., 1987. Laser diffraction spectrometry: Fraunhofer diffraction versus Mie scattering. *Part. Charact.* 4:14–19.
- Deng, X., and Underwood, M.B., 2001. Abundance of smectite and the location of a plate-boundary fault, Barbados accretionary prism. *Geol. Soc. Am. Bull.*, 113(4):495–507. [doi:10.1130/0016-7606\(2001\)113<0495:AOSATL>2.0.CO;2](https://doi.org/10.1130/0016-7606(2001)113<0495:AOSATL>2.0.CO;2)
- Expedition 315 Scientists, 2009a. Expedition 315 Site C0001. *In* Kinoshita, M., Tobin, H., Ashi, J., Kimura, G., Lallemand, S., Screamton, E.J., Curewitz, D., Masago, H., Moe, K.T., and the Expedition 314/315/316 Scientists, *Proc. IODP*, 314/315/316: Washington, DC (Integrated Ocean Drilling Program Management International, Inc.). [doi:10.2204/iodp.proc.314315316.123.2009](https://doi.org/10.2204/iodp.proc.314315316.123.2009)
- Expedition 315 Scientists, 2009b. Expedition 315 Site C0002. *In* Kinoshita, M., Tobin, H., Ashi, J., Kimura, G., Lallemand, S., Screamton, E.J., Curewitz, D., Masago, H., Moe, K.T., and the Expedition 314/315/316 Scientists, *Proc. IODP*, 314/315/316: Washington, DC (Integrated Ocean Drilling Program Management International, Inc.). [doi:10.2204/iodp.proc.314315316.124.2009](https://doi.org/10.2204/iodp.proc.314315316.124.2009)
- Expedition 316 Scientists, 2009a. Expedition 316 Site C0004. *In* Kinoshita, M., Tobin, H., Ashi, J., Kimura, G., Lallemand, S., Screamton, E.J., Curewitz, D., Masago, H., Moe, K.T., and the Expedition 314/315/316 Scientists, *Proc. IODP*, 314/315/316: Washington, DC (Integrated Ocean Drilling Program Management International, Inc.). [doi:10.2204/iodp.proc.314315316.133.2009](https://doi.org/10.2204/iodp.proc.314315316.133.2009)
- Expedition 316 Scientists, 2009b. Expedition 316 Site C0006. *In* Kinoshita, M., Tobin, H., Ashi, J., Kimura, G., Lallemand, S., Screamton, E.J., Curewitz, D., Masago, H., Moe, K.T., and the Expedition 314/315/316 Scientists, *Proc. IODP*, 314/315/316: Washington, DC (Integrated Ocean Drilling Program Management International, Inc.). [doi:10.2204/iodp.proc.314315316.134.2009](https://doi.org/10.2204/iodp.proc.314315316.134.2009)
- Expedition 316 Scientists, 2009c. Expedition 316 Site C0007. *In* Kinoshita, M., Tobin, H., Ashi, J., Kimura, G., Lallemand, S., Screamton, E.J., Curewitz, D., Masago, H., Moe, K.T., and the Expedition 314/315/316 Scientists, *Proc. IODP*, 314/315/316: Washington, DC (Integrated Ocean Drilling Program Management International, Inc.). [doi:10.2204/iodp.proc.314315316.135.2009](https://doi.org/10.2204/iodp.proc.314315316.135.2009)
- Expedition 316 Scientists, 2009d. Expedition 316 Site C0008. *In* Kinoshita, M., Tobin, H., Ashi, J., Kimura, G., Lallemand, S., Screamton, E.J., Curewitz, D., Masago, H., Moe, K.T., and the Expedition 314/315/316 Scientists, *Proc. IODP*, 314/315/316: Washington, DC (Integrated Ocean Drilling Program Management International, Inc.). [doi:10.2204/iodp.proc.314315316.136.2009](https://doi.org/10.2204/iodp.proc.314315316.136.2009)
- Expedition 319 Scientists, 2010. Expedition 319 summary. *In* Saffer, D., McNeill, L., Byrne, T., Araki, E., Toczko, S., Eguchi, N., Takahashi, K., and the Expedition 319 Scientists, *Proc. IODP*, 319: Tokyo (Integrated Ocean Drilling Program Management International, Inc.). [doi:10.2204/iodp.proc.319.101.2010](https://doi.org/10.2204/iodp.proc.319.101.2010)
- Folk, R.L., 1966. A review of grain-size parameters. *Sedimentology*, 6(2):73–93. [doi:10.1111/j.1365-3091.1966.tb01572.x](https://doi.org/10.1111/j.1365-3091.1966.tb01572.x)
- Folk, R.L., and Ward, W.C., 1957. Brazos River bar [Texas]: a study in the significance of grain size parameters. *J. Sediment. Res.*, 27(1):3–26. <http://jsedres.sepmon-line.org/cgi/content/abstract/27/1/3>

- Gulick, S.P.S., Bangs, N.L.B., Moore, G.F., Ashi, J., Martin, K.M., Sawyer, D.S., Tobin, H.J., Kuramoto, S., and Taira, A., 2010. Rapid forearc basin uplift and megasplay fault development from 3D seismic images of Nankai margin off Kii Peninsula, Japan. *Earth Planet. Sci. Lett.*, 300(1–2):55–62. doi:10.1016/j.epsl.2010.09.034
- Jones, K.P.N., McCave, I.N., and Weaver, P.P.E., 1992. Textural and dispersal patterns of thick mud turbidites from the Madeira Abyssal Plain. *Mar. Geol.*, 107(3):149–173. doi:10.1016/0025-3227(92)90165-E
- Kawamura, K., Kanamatsu, T., Kinoshita, M., Saito, S., Shibata, T., Fujino, K., Misawa, A., and Burmeister, K.C., 2010. Redistribution of sediments by submarine landslides on the eastern Nankai accretionary prism. In Mosher, D.C., Moscardelli, L., Baxter, C.D.P., Urgeles, R., Shipp, R.C., Chaytor, J.D., and Lee, H.J. (Eds.), *Submarine Mass Movements and Their Consequences*. Adv. Nat. Technol. Hazards Res., 28:313–322. doi:10.1007/978-90-481-3071-9\_26
- Kawamura, K., Ogawa, Y., Anma, R., Yokoyama, S., Kawakami, S., Dilek, Y., Moore, G.F., Hirano, S., Yamaguchi, A., Sasaki, T., and the YK05-08 Leg 2 and YK06-02 Shipboard Scientific Parties, 2009. Structural architecture and active deformation of the Nankai accretionary prism, Japan: submersible survey results from the Tenryu submarine canyon. *GSA Bull.*, 121(11–12):1629–1646. doi:10.1130/B26219.1
- Konert, M., and Vandenberghe, J., 1997. Comparison of laser grain size analysis with pipette and sieve analysis: a solution for the underestimation of the clay fraction. *Sedimentology*, 44(3):523–535. doi:10.1046/j.1365-3091.1997.d01-38.x
- Kopf, A., and Brown, K.M., 2003. Friction experiments on saturated sediments and their implications for the stress state of the Nankai and Barbados subduction thrusts. *Mar. Geol.*, 202(3–4):193–210. doi:10.1016/S0025-3227(03)00286-X
- Loizeau, J.-L., Arbouille, D., Santiago, S., and Vernet, J.-P., 1994. Evaluation of a wide range laser diffraction grain size analyser for use with sediments. *Sedimentology*, 41(2):353–361. doi:10.1111/j.1365-3091.1994.tb01410.x
- Lucchi, R., and Camerlenghi, A., 1993. Upslope turbidite sedimentation on the southeastern flank of the Mediterranean Ridge. *Boll. Oceanol. Teor. Appl.*, 11:3–25.
- Martin, K.M., Gulick, S.P.S., Bangs, N.L.B., Moore, G.F., Ashi, J., Park, J.-O., Kuramoto, S., and Taira, A., 2010. Possible strain partitioning structure between the Kumano fore-arc basin and the slope of the Nankai Trough accretionary prism. *Geochem., Geophys., Geosyst.*, 11:Q0AD02–Q0AD16. doi:10.1029/2009GC002668
- Moore, G.F., Bangs, N.L., Taira, A., Kuramoto, S., Pangborn, E., and Tobin, H.J., 2007. Three-dimensional splay fault geometry and implications for tsunami generation. *Science*, 318(5853):1128–1131. doi:10.1126/science.1147195
- Moore, G.F., Park, J.-O., Bangs, N.L., Gulick, S.P., Tobin, H.J., Nakamura, Y., Sato, S., Tsuji, T., Yoro, T., Tanaka, H., Uraki, S., Kido, Y., Sanada, Y., Kuramoto, S., and Taira, A., 2009. Structural and seismic stratigraphic framework of the NanTroSEIZE Stage 1 transect. In Kinoshita, M., Tobin, H., Ashi, J., Kimura, G., Lallemand, S., Screaton, E.J., Curewitz, D., Masago, H., Moe, K.T., and the Expedition 314/315/316 Scientists, *Proc. IODP, 314/315/316*: Washington, DC (Integrated Ocean Drilling Program Management International, Inc.). doi:10.2204/iodp.proc.314315316.102.2009
- Moore, G.F., Taira, A., Klaus, A., Becker, L., Boeckel, B., Cragg, B.A., Dean, A., Fergusson, C.L., Henry, P., Hirano, S., Hisamitsu, T., Hunze, S., Kastner, M., Maltman, A.J., Morgan, J.K., Murakami, Y., Saffer, D.M., Sánchez-Gómez, M., Screaton, E.J., Smith, D.C., Spivack, A.J., Steurer, J., Tobin, H.J., Ujiie, K., Underwood, M.B., and Wilson, M., 2001. New insights into deformation and fluid flow processes in the Nankai Trough accretionary prism: results of Ocean Drilling Program Leg 190. *Geochem., Geophys., Geosyst.*, 2(10):1058–1079. doi:10.1029/2001GC000166
- Morley, C.K., 2009. Growth of folds in a deep-water setting. *Geosphere*, 5(2):59–89. doi:10.1130/GES00186.1
- Park, J.-O., Tsuru, T., Kodaira, S., Cummins, P.R., and Kaneda, Y., 2002. Splay fault branching along the Nankai subduction zone. *Science*, 297(5584):1157–1160. doi:10.1126/science.1074111
- Rothwell, R.G., Weaver, P.P.E., Hodgkinson, R.A., Pratt, C.E., Styzen, M.J., and Higgs, N.C., 1994. Clayey nannofossil ooze turbidites and hemipelagites at Sites 834 and 835 (Lau Basin, southwest Pacific). In Hawkins, J., Parson, L., Allan, J., et al., *Proc. ODP, Sci. Results*, 135: College Station, TX (Ocean Drilling Program), 101–130. doi:10.2973/odp.proc.sr.135.108.1994
- Screaton, E.J., Kimura, G., Curewitz, D., and the Expedition 316 Scientists, 2009a. Expedition 316 summary. In Kinoshita, M., Tobin, H., Ashi, J., Kimura, G., Lallemand, S., Screaton, E.J., Curewitz, D., Masago, H., Moe, K.T., and the Expedition 314/315/316 Scientists, *Proc. IODP, 314/315/316*: Washington, DC (Integrated Ocean Drilling Program Management International, Inc.). doi:10.2204/iodp.proc.314315316.131.2009
- Screaton, E., Kimura, G., Curewitz, D., Moore, G., Fabbri, O., Fergusson, C., Girault, F., Goldsby, D., Harris, R., Inagaki, F., Jiang, T., Kitamura, Y., Knuth, M., Li, C.-F., Claesson Liljedahl, L., Louis, L., Milliken, K., Nicholson, U., Riedinger, N., Sakaguchi, A., Solomon, E., Strasser, M., Su, X., Tsutsumi, A., Yamaguchi, A., Ujiie, K., and Zhao, X., 2009b. Interactions between deformation and fluids in the frontal thrust region of the NanTroSEIZE transect offshore the Kii Peninsula, Japan: results from IODP Expedition 316 Sites C0006 and C0007. *Geochem., Geophys., Geosyst.*, 10:Q0AD01–Q0AD14. doi:10.1029/2009GC002713
- Spencer, D.W., 1963. The interpretation of grain size distribution curves of clastic sediments. *J. Sediment. Petrol.*, 33(1):180–190. doi:10.1306/74D70DF8-2B21-11D7-8648000102C1865D
- Spinelli, G.A., and Underwood, M.B., 2004. Character of sediments entering the Costa Rica subduction zone: implications for partitioning of water along the plate interface. *Isl. Arc*, 13(3):432–451. doi:10.1111/j.1440-1738.2004.00436.x

- Stow, D.A.V., and Wetzel, A., 1990. Hemiturbidite: a new type of deep-water sediment. *In* Cochran, J.R., Stow, D.A.V., et al., *Proc. ODP, Sci. Results*, 116: College Station, TX (Ocean Drilling Program), 25–34. [doi:10.2973/odp.proc.sr.116.152.1990](https://doi.org/10.2973/odp.proc.sr.116.152.1990)
- Strasser, M., Moore, G.F., Kimura, G., Kitamura, Y., Kopf, A.J., Lallemand, S., Park, J.-O., Screaton, E.J., Su, X., Underwood, M.B., and Zhao, X., 2009. Origin and evolution of a splay fault in the Nankai accretionary wedge. *Nat. Geosci.*, 2(9):648–652. [doi:10.1038/ngeo609](https://doi.org/10.1038/ngeo609)
- Strasser, M., Moore, G.F., Kimura, G., Kopf, A.J., Underwood, M.B., Guo, J., and Screaton, E.J., 2011. Slumping and mass-transport deposition in the Nankai forearc: evidence from IODP drilling and 3-D reflection seismic data. *Geochem., Geophys., Geosyst.*, 12:Q0AD13–Q0AD36. [doi:10.1029/2010GC003431](https://doi.org/10.1029/2010GC003431)
- Sun, D., Bloemendal, J., Rea, D.K., Vandenberghe, J., Jiang, F., An, Z.S., and Su, R., 2002. Grain-size distribution function of polymodal sediments in hydraulic and aeolian environments, and numerical partitioning of the sedimentary components. *Sediment. Geol.*, 152(3–4):263–277. [doi:10.1016/S0037-0738\(02\)00082-9](https://doi.org/10.1016/S0037-0738(02)00082-9)
- Sutherland, R.A., and Lee, C.-T., 1994. Discrimination between coastal subenvironments using textural characteristics. *Sedimentology*, 41(6):1133–1145. [doi:10.1111/j.1365-3091.1994.tb01445.x](https://doi.org/10.1111/j.1365-3091.1994.tb01445.x)
- Syvitski, J.P.M. (Ed.), 1991. *Principles, Methods, and Application of Particle Size Analysis*: Cambridge (Cambridge Univ. Press).
- Syvitski, J.P.M., LeBlanc, K.W.G., and Asprey, K.W., 1991. Interlaboratory, interinstrument calibration experiment. *In* Syvitski, J.P.M. (Ed.), *Principles, Methods and Application of Particle Size Analysis*: Cambridge (Cambridge Univ. Press), 174–194. [doi:10.1017/CBO9780511626142.016](https://doi.org/10.1017/CBO9780511626142.016)
- Tobin, H.J., and Kinoshita, M., 2006. NanTroSEIZE: the IODP Nankai Trough Seismogenic Zone Experiment. *Sci. Drill.*, 2:23–27. [doi:10.2204/iodp.sd.2.06.2006](https://doi.org/10.2204/iodp.sd.2.06.2006)
- Tobin, H., Kinoshita, M., Ashi, J., Lallemand, S., Kimura, G., Screaton, E.J., Moe, K.T., Masago, H., Curewitz, D., and the Expedition 314/315/316 Scientists, 2009a. NanTroSEIZE Stage 1 expeditions: introduction and synthesis of key results. *In* Kinoshita, M., Tobin, H., Ashi, J., Kimura, G., Lallemand, S., Screaton, E.J., Curewitz, D., Masago, H., Moe, K.T., and the Expedition 314/315/316 Scientists, *Proc. IODP*, 314/315/316: Washington, DC (Integrated Ocean Drilling Program Management International, Inc.). [doi:10.2204/iodp.proc.314315316.101.2009](https://doi.org/10.2204/iodp.proc.314315316.101.2009)
- Tobin, H., Kinoshita, M., Moe, K.T., and the Expedition 314 Scientists, 2009b. Expedition 314 summary. *In* Kinoshita, M., Tobin, H., Ashi, J., Kimura, G., Lallemand, S., Screaton, E.J., Curewitz, D., Masago, H., Moe, K.T., and the Expedition 314/315/316 Scientists, *Proc. IODP*, 314/315/316: Washington, DC (Integrated Ocean Drilling Program Management International, Inc.). [doi:10.2204/iodp.proc.314315316.111.2009](https://doi.org/10.2204/iodp.proc.314315316.111.2009)
- Udden, J.A., 1914. Mechanical composition of clastic sediments. *Geol. Soc. Am. Bull.*, 25:655–744.
- Underwood, M., Basu, N., Steurer, J., and Udas, S., 2003. Data report: normalization factors for semiquantitative X-ray diffraction analysis, with application to DSDP Site 297, Shikoku Basin. *In* Mikada, H., Moore, G.F., Taira, A., Becker, K., Moore, J.C., and Klaus, A. (Eds.), *Proc. ODP, Sci. Results*, 190/196: College Station, TX (Ocean Drilling Program), 1–28. [doi:10.2973/odp.proc.sr.190196.203.2003](https://doi.org/10.2973/odp.proc.sr.190196.203.2003)
- Underwood, M.B., Saito, S., Kubo, Y., and the Expedition 322 Scientists, 2010. Expedition 322 summary. *In* Saito, S., Underwood, M.B., Kubo, Y., and the Expedition 322 Scientists, *Proc. IODP*, 322: Tokyo (Integrated Ocean Drilling Program Management International, Inc.). [doi:10.2204/iodp.proc.322.101.2010](https://doi.org/10.2204/iodp.proc.322.101.2010)
- Weedon, G.P., and McCave, I.N., 1991. Mud turbidites from the Oligocene and Miocene Indus Fan at Sites 722 and 731 on the Owen Ridge. *In* Prell, W.L., Niitsuma, N., et al., *Proc. ODP, Sci. Results*, 117: College Station, TX (Ocean Drilling Program), 215–220. [doi:10.2973/odp.proc.sr.117.140.1991](https://doi.org/10.2973/odp.proc.sr.117.140.1991)
- Wentworth, C.K., 1922. A scale of grade and class terms for clastic sediments. *J. Geol.*, 30(5):377–392. [doi:10.1086/622910](https://doi.org/10.1086/622910)

**Initial receipt:** 5 October 2010

**Acceptance:** 7 September 2011

**Publication:** 7 November 2011

**MS 314315316-207**

**Figure F1.** A. Map of the Nankai Trough study area including the Nankai Trough Seismogenic Zone Experiment (NanTroSEIZE) Stage 1 drilling transect (red line) in the Kumano Basin area, Japan. Inset shows overall plate tectonic setting. B. Regional long seismic reflection depth line (after Park et al., 2002) with drilled NanTroSEIZE Stage 1 sites and major interpreted tectonic features. After Tobin et al. (2009a) and Strasser et al. (2009). VE = vertical exaggeration.

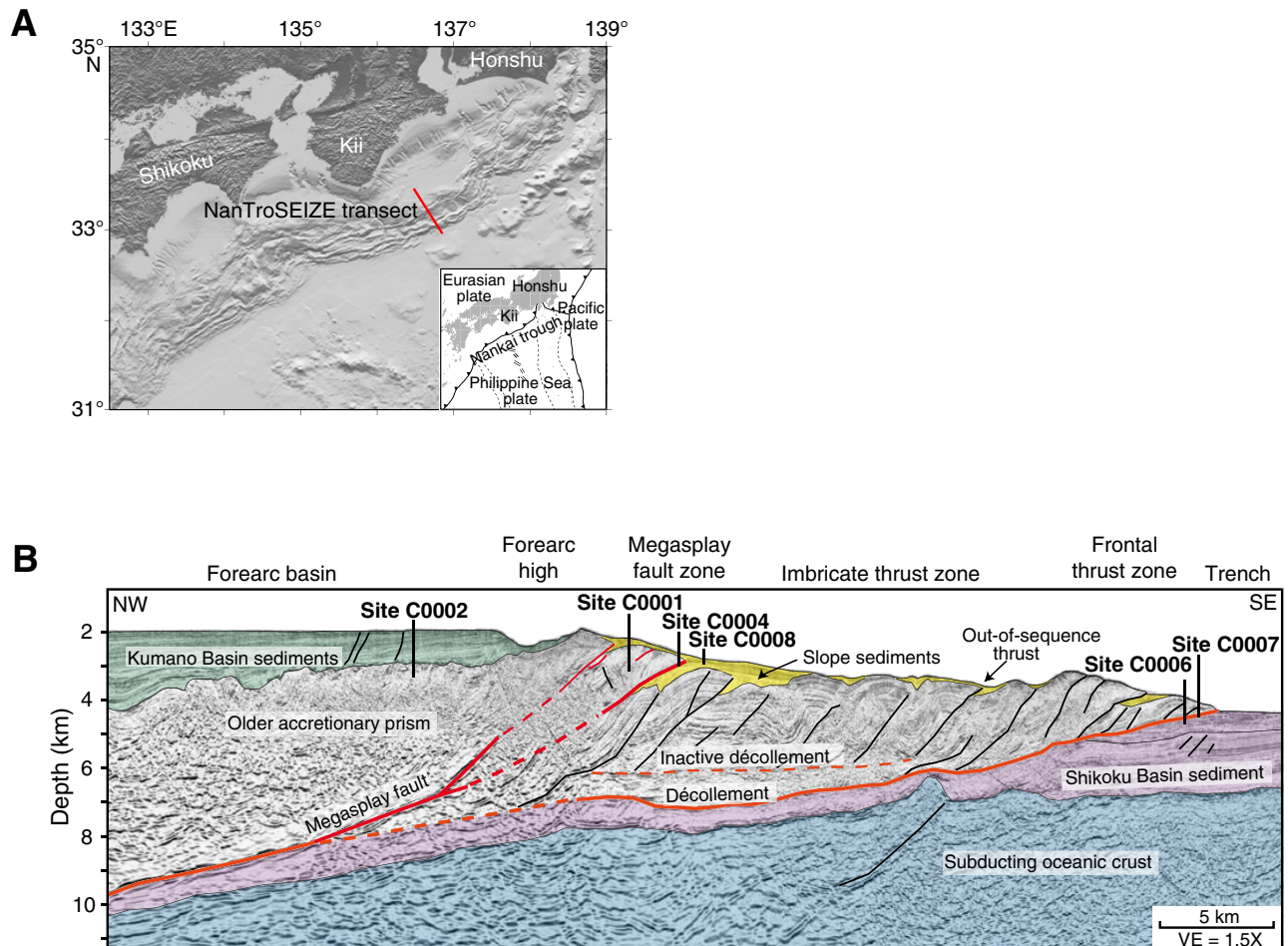


**Figure F2.** Lithologic column and major lithostratigraphic units of Site C0001, as identified during NanTro-SEIZE Stage 1 drilling (see the “Expedition 315 Site C0001” chapter [Expedition 315 Scientists, 2009a]).

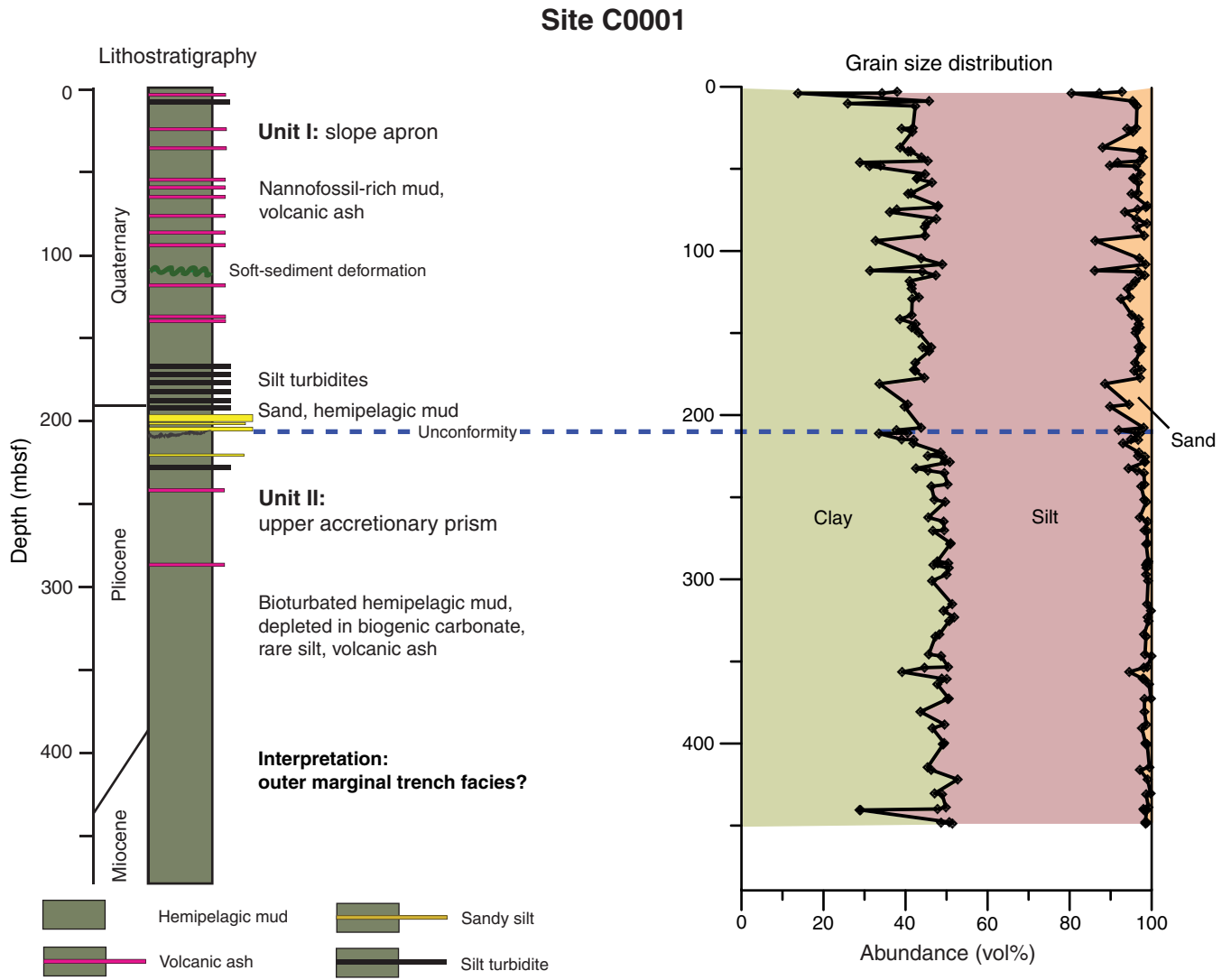


**Figure F3.** Lithologic column and major lithostratigraphic units of Site C0002, as identified during NanTro-SEIZE Stage 1 drilling (see the “[Expedition 315 Site C0002](#)” chapter [Expedition 315 Scientists, 2009b]).

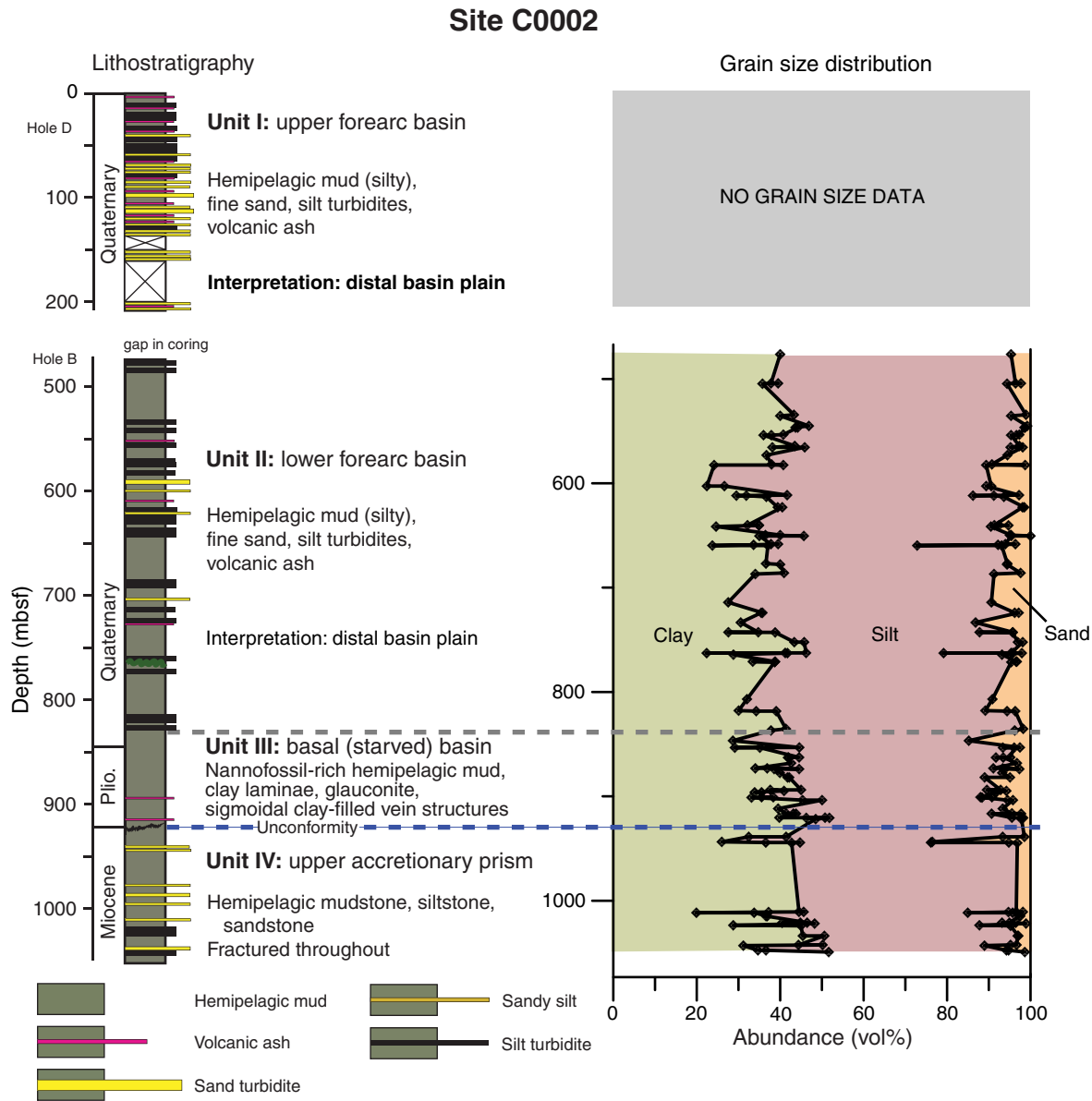


**Figure F4.** Lithologic column and major lithostratigraphic units of Site C0004, as identified during NanTro-SEIZE Stage 1 drilling (see the “[Expedition 316 Site C0004](#)” chapter [Expedition 316 Scientists, 2009a]).

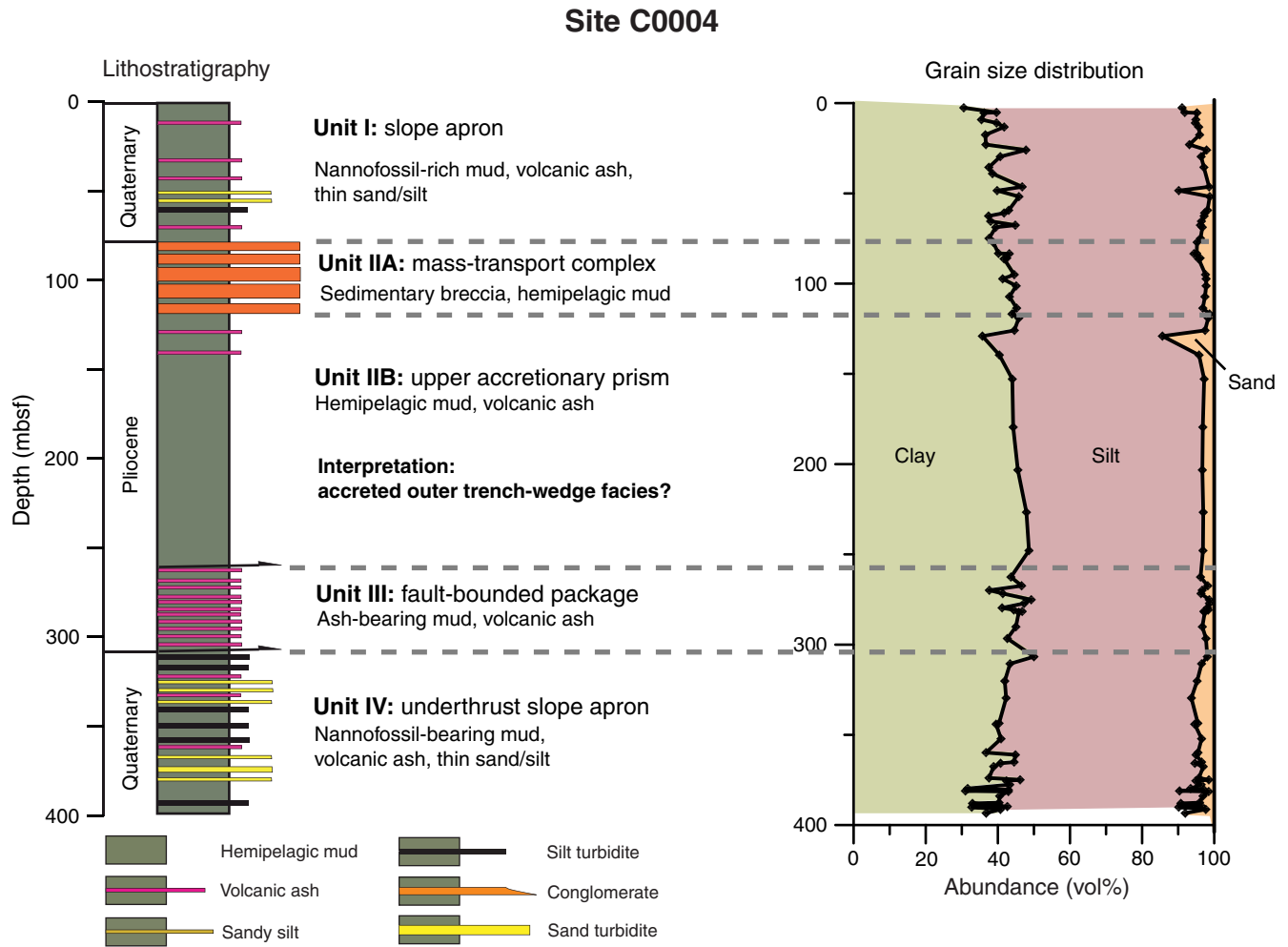


**Figure F5.** Lithologic column and major lithostratigraphic units of Site C0006, as identified during NanTro-SEIZE Stage 1 drilling (see the “[Expedition 316 Site C0006](#)” chapter [Expedition 316 Scientists, 20009b]).

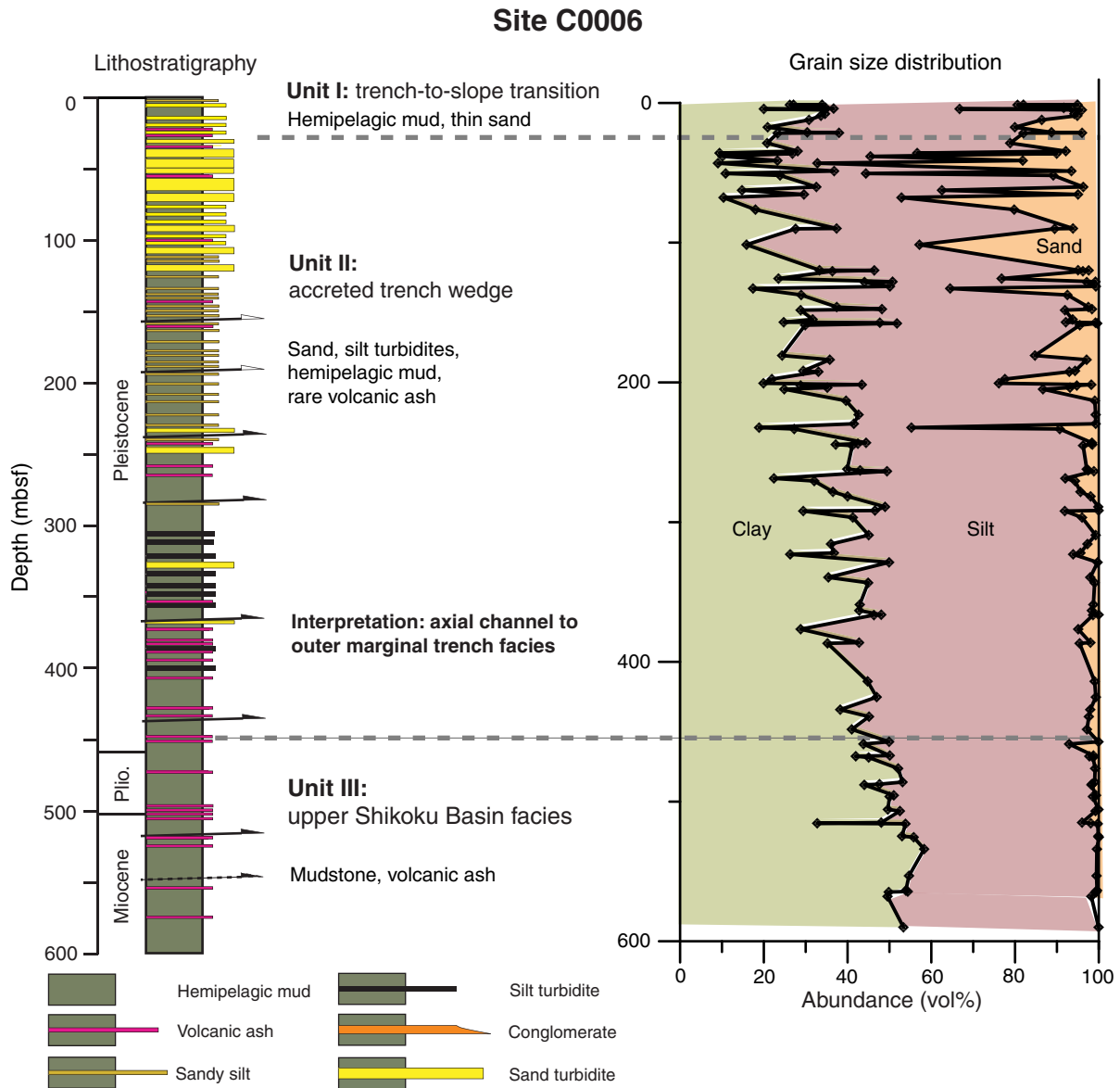


**Figure F6.** Lithologic column and major lithostratigraphic units of Site C0008, as identified during NanTro-SEIZE Stage 1 drilling (see the “Expedition 316 Site C0008” chapter [Expedition 316 Scientists, 2009d]).

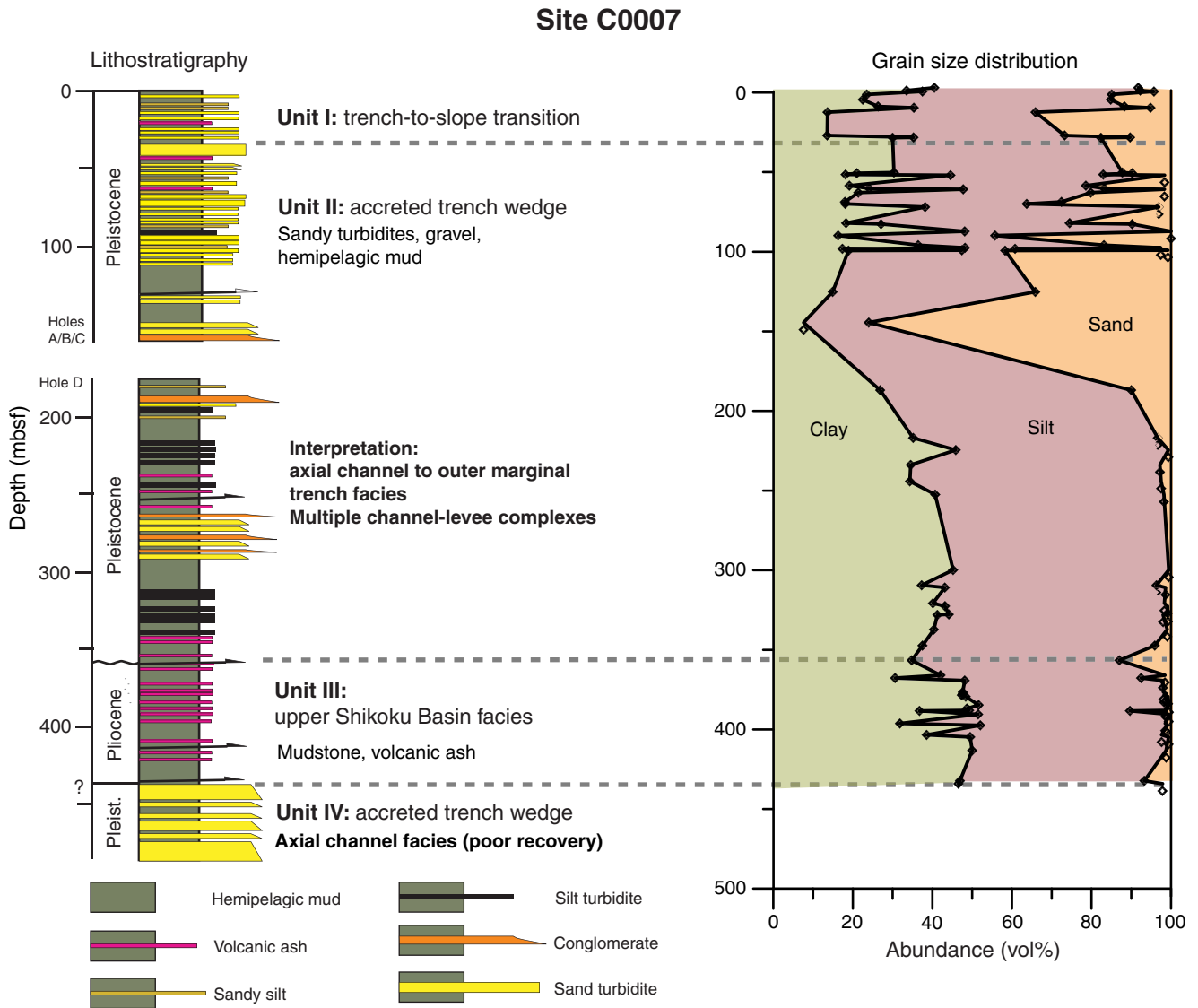


**Figure F7.** Lithologic column and major lithostratigraphic units of Site C0007, as identified during NanTro-SEIZE Stage 1 drilling (see the “[Expedition 316 Site C0007](#)” chapter [Expedition 316 Scientists, 2009c]).

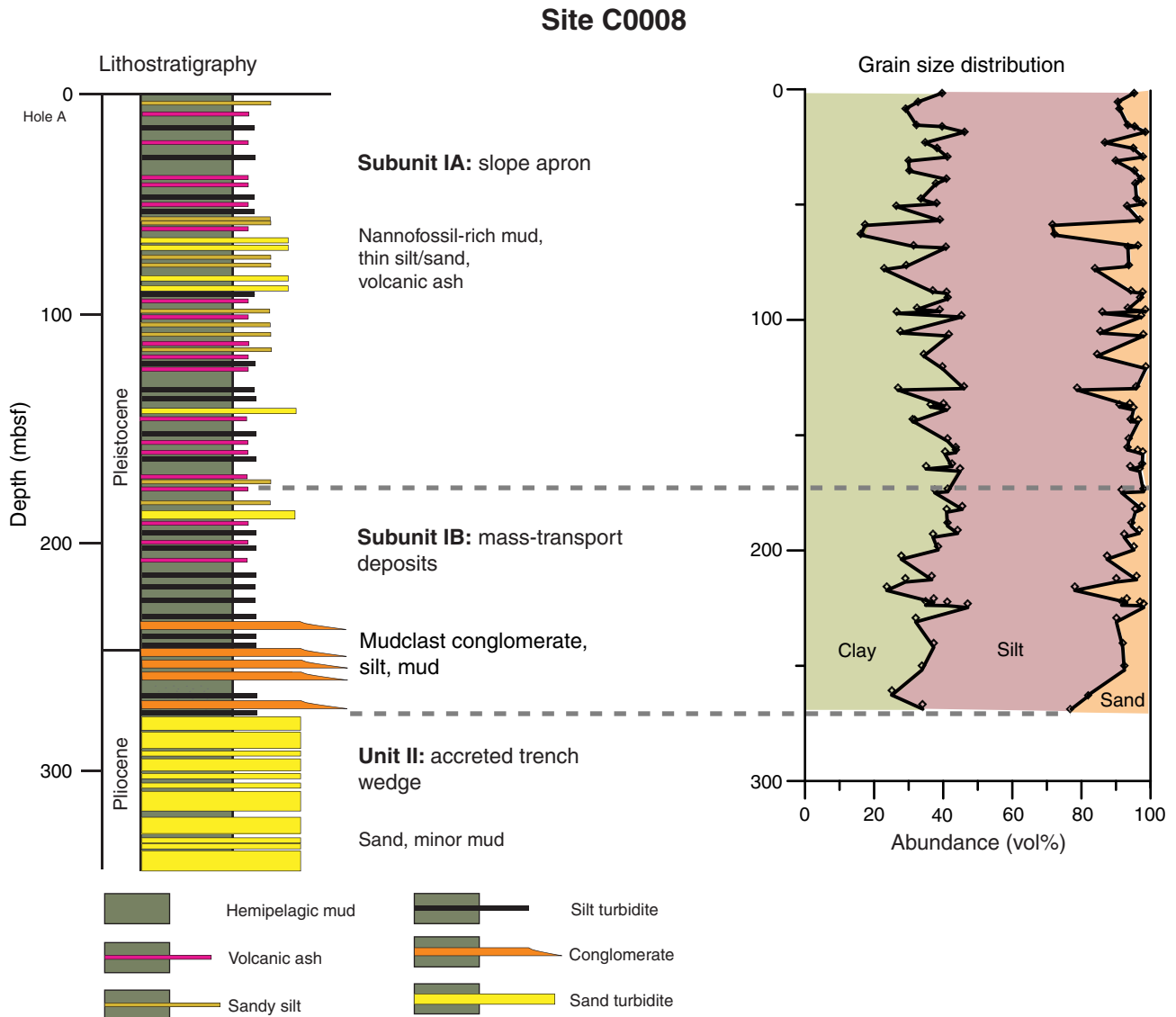


**Figure F8.** Mean of grain size for samples collected at upper slope/forearc basin/Kumano Basin edge fault zone Sites C0001 and C0002, mid-slope Sites C0004 and C0008, and lowermost slope/prism toe/frontal thrust zone Sites C0006 and C0007. See Figures F2, F3, F4, F5, F6, and F7 for corresponding lithologic information and clay-silt-sand distribution.

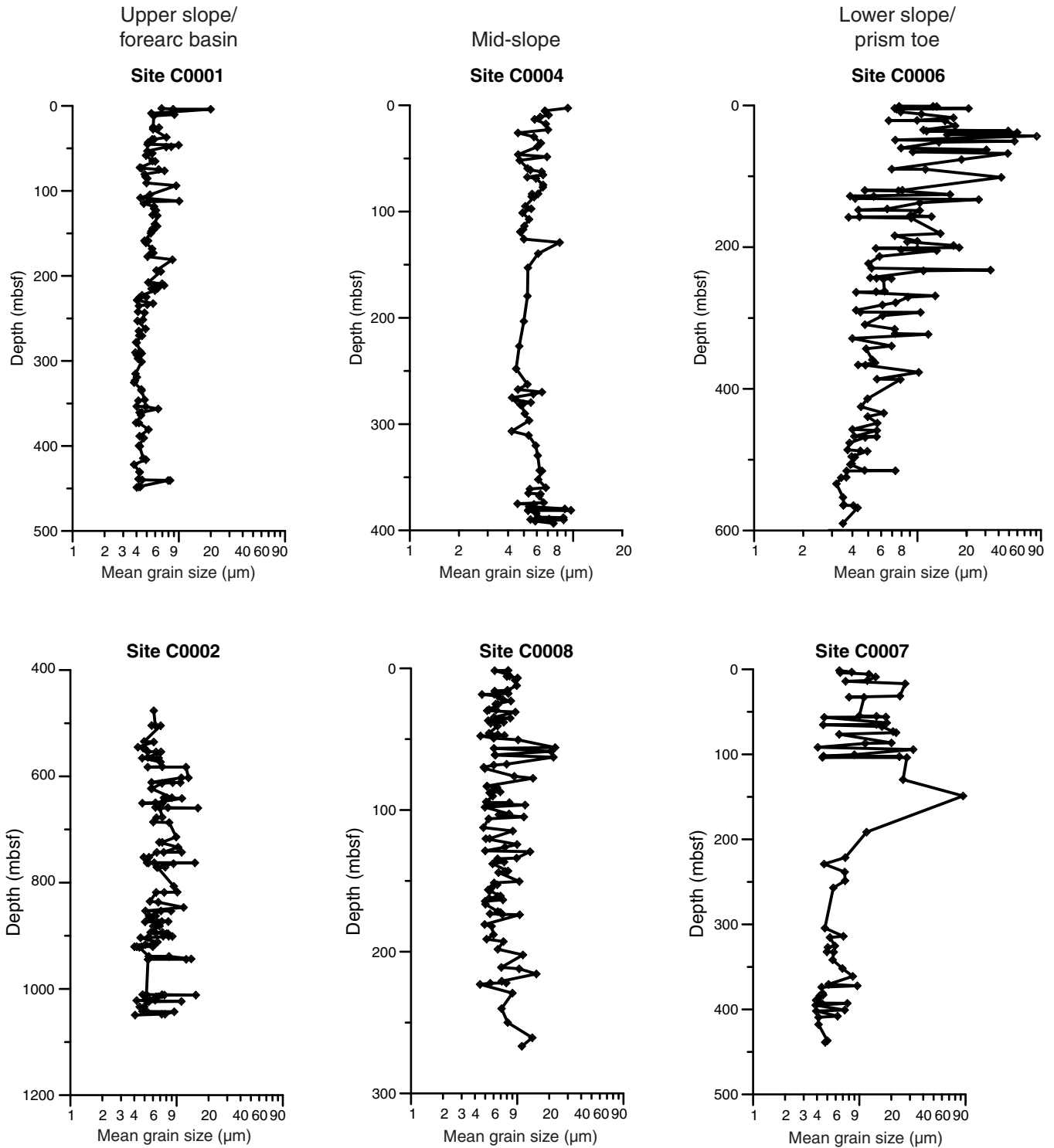




**Figure F9.** Grain size distribution patterns of 16 subsamples processed as two batches of eight (Sample 315-C0001H-10R-5, 10–16 cm). **A.** 30 min of disaggregation time. **B.** 120 min of disaggregation time.

